

Skyrmion states in disk geometry

Thomas Brian Winkler^{1,*}, Kai Litzius², Andrea de Lucia,
Markus Weißenhofer³, Hans Fangohr^{4,5,6,†} and Mathias Kläui^{1‡}

Institute of Physics, Johannes Gutenberg Universität,

Staudinger Weg 7. 55122 Mainz, Germany

Department of Materials Science and Engineering,

Massachusetts Institute of Technology, Cambridge, MA, USA

Fachbereich Physik, Universität Konstanz,

Universitätsstraße 10 78464 Konstanz, Germany

Max-Planck Institute for Structure and Dynamics of Matter,

Luruper Chaussee 149, 22761 Hamburg, Germany

European XFEL, Holzkoppel 4, 22869 Schenefeld, Germany and

University of Southampton, Highfield, SO17 1BJ, United Kingdom

(Dated: November 10, 2021)

Abstract

In this work we explore the stability of magnetic skyrmions confined in a disk geometry by analyzing how to switch a skyrmionic state in a circular disk into a uniformly magnetized state when applying an external magnetic field. The technologically highly relevant energy barrier between the skyrmion state and the uniformly magnetized state is a key parameter needed for lifetime calculations. In an infinite sample this relates to the out-of-plane *rupture field* against the skyrmion core direction, while in confined geometries the topological charge can also be changed by interactions with the sample edges.

We find that, annihilating a skyrmion with an applied field in the direction of the core magnetization - we call this *expulsion* - , the energy barrier to the uniform state is generally around one order of magnitude lower than the annihilation via the rupture of the core in the disk center, which is observed when the applied field is acting in the direction opposite to the core magnetization. For the latter case a Bloch point needs to be nucleated to change the topological charge to zero. We find that the former case can be realistically calculated using micromagnetic simulations, but the annihilation via rupture, involving a Bloch point, needs to be calculated with the Heisenberg model because the high magnetization gradients present during the annihilation process cannot be accurately described within the micromagnetic framework.

* twinkler@uni-mainz.de

† hans.fangohr@mpsd.mpg.de

‡ Klaeui@uni-mainz.de

I. INTRODUCTION

Magnetic skyrmions [1, 2] can be found in spin patterns of magnetic systems with broken inversion symmetry, e.g. in thin magnetic films with an interfacial Dzyaloshinskii-Moriya interaction (DMI) [3, 4]. They are quasi-particles, and their properties make them promising candidates for next generation non-conventional computing and storage devices such as probabilistic computing [5, 6] or racetrack-memory [7, 8]. For such devices, controlled nucleation [9–11], annihilation [12] and movement [13, 14] of skyrmions is generally required while the existence or absence of a skyrmion defines the logical bit. Skyrmions can also be used in so called bit-patterned media (BPM) [15], where magnetic disk structures in the nm-range are lithographically patterned into a storage medium. That way, the superparamagnetic limits of conventional magnetic storage devices can potentially be mitigated to some extent [16]. Apart from their potential for applications, skyrmions show interesting physical behavior, such as the skyrmion hall angle [17, 18]. Some of these effects may arise due to their quasi-particle nature and their topological stabilization. Recent work has shown pulse-induced nucleation of skyrmions or the nucleation at pinning sites [9–11, 19], but the nucleation process is still not well understood since it is a process on and below the timescale of nanoseconds. However, a nucleation of skyrmions is possible by applying in-plane (IP) fields, as shown in various experiments [19]. Likewise, the lifetime of skyrmions has been investigated [6, 20] in the past, since this is an important parameter for device applications. However, the energy barrier between the skyrmionic and the uniformly magnetized state remains a mostly elusive, yet required parameter for lifetime calculations and poses a major challenge for predicting the stability of skyrmions in potential new devices. In our set-up it is related to the annihilation field H^* , that is needed to transform the skyrmion state into the uniformly magnetized state via an out-of-plane (OOP) field. The field will be applied in both directions; in the skyrmion core direction and against the skyrmion core. The life time also depends also on temperature and the attempt frequency, according to the Arrhenius-Neél law [12, 21, 22]. To model future devices effectively, it is important to know how a magnetic system will behave under certain conditions and how magnetic parameters influence this behavior. This approach is important to avoid inefficient "trial-and-error" fabrications. Furthermore, the energy barrier of skyrmionic states is of interest to understand the physics of topological protected spin structures and how much their topology can contribute to their enhanced stability. Moreover, it is important to know the limitations of a chosen simulation model.

In this work we investigate the dependence of H^* on all key magnetic material parameters, namely the exchange constant, the DMI strength, the anisotropy constant and the saturation magnetization. We vary the disk size to analyze the dependence of the annihilation field on the geometry present and we ascertain the computational models required for robust analysis of the value of the annihilation field. Using a multiscale model we demonstrate where the Heisenberg (HB) model is required and where conventional micromagnetic approaches are sufficient.

II. COMPUTATIONAL MODELS

We use two different computational methods to simulate the physics of the system: the micromagnetic model (MM) which assumes that the magnetization of the sample is a vector field defined on a continuous region in space, and a Heisenberg model which represents the individual magnetic moments of individual atoms.

A. Micromagnetics

The micromagnetic (MM) model [23] describes the magnetization using partial differential equations (PDEs) derived from classical field theory. While these PDEs have to be discretized and solved numerically, we can choose a discretization cell size that is significantly larger than the spacing of the actual magnetic moments. For this reason one is able to simulate the behavior of experimentally relevant mesoscopic samples. The MM approach is generally not valid when the system shows strong spatial variations of the spin texture. This is the case for small skyrmions or when dynamic processes involving Bloch point [24] type configurations occur. Then the spatial derivative of the MM magnetization function can diverge: It is an assumption of the numerical micromagnetic model that the magnetization vector field changes slowly as a function of space [23]. For example, it has been shown that the micromagnetic exchange energy significantly overestimates the exchange energy of a spin wave system with a wavelength of the order of the cell size [25].

B. Heisenberg model

The HB model [26] represents the magnetization through dipole moments that are associated with the discrete magnetic moments in the crystal lattice.

The HB model is a more accurate description of the sample than the micromagnetic model: we can simulate every single magnetic moment and the HB model makes no approximations regarding the spatial variation in the magnetic moments.

However, due to the larger computational cost, the material volume which can be simulated in the HB model is limited [27].

C. Hamiltonians

We next describe the Hamiltonians for the discretized micromagnetic (MM) model and the Heisenberg (HB) model.

The exchange energy E_{xc} for the Hamiltonian for the HB and the MM model are given by

$$E_{xc,HB} = -\frac{1}{2} \sum_{i,j} J_{i,j} \mathbf{S}_i \cdot \mathbf{S}_j \quad (1)$$

$$E_{xc,MM} = \frac{A}{M_S^2} \int_V dr |\nabla \mathbf{M}(\mathbf{r})|^2 \quad (2)$$

with \mathbf{S}_i the spin vector at position \mathbf{r}_i , and $|\mathbf{S}_i| = \mu_i$ its magnetic moment, $J_{i,j}$ the exchange coupling constant between spin i and spin j . In the MM model, $\mathbf{M}(\mathbf{r})$ is the magnetization at point \mathbf{r} with the saturation magnetization $M_S = |\mathbf{M}|$, and A the exchange stiffness.

The conversion between the models can be realized using $\mu = a^3 M_S$ and $A = J \cdot \mathbf{S}^2 \cdot c_s / a$ with a the lattice constant and c_s the number of nearest neighbors in the lattice [28]. To describe the Dzyaloshinskii-Moriya Interaction (DMI), the energy terms in the two models are:

$$E_{DMI,HB} = \frac{1}{2} \sum_{i,j} \mathbf{D}_{i,j} \cdot \mathbf{S}_i \times \mathbf{S}_j \quad (3)$$

$$E_{DMI,MM} = \frac{A}{M_S^2} \int_V dV D_a \mathbf{M}(\mathbf{r}) \cdot (\nabla \times \mathbf{M}(\mathbf{r})) \quad (4)$$

with D the DMI interaction strength, $\mathbf{D} = D \mathbf{r}_{i,j} \times \mathbf{e}_z$ for interfacial DMI and $D_a = -D/a^2$ with $\mathbf{r}_{i,j}$ the distance of two neighbored spins and \mathbf{e}_z the unit vector in z-direction. For Zeeman and the uniaxial anisotropy energy, the terms for HB and a discretized MM model are equivalent, hence we provide only the HB description:

$$E_{Zeeman} = -\mu_0 \sum_i \mathbf{H}_{ext} \cdot \mathbf{S}_i \quad (5)$$

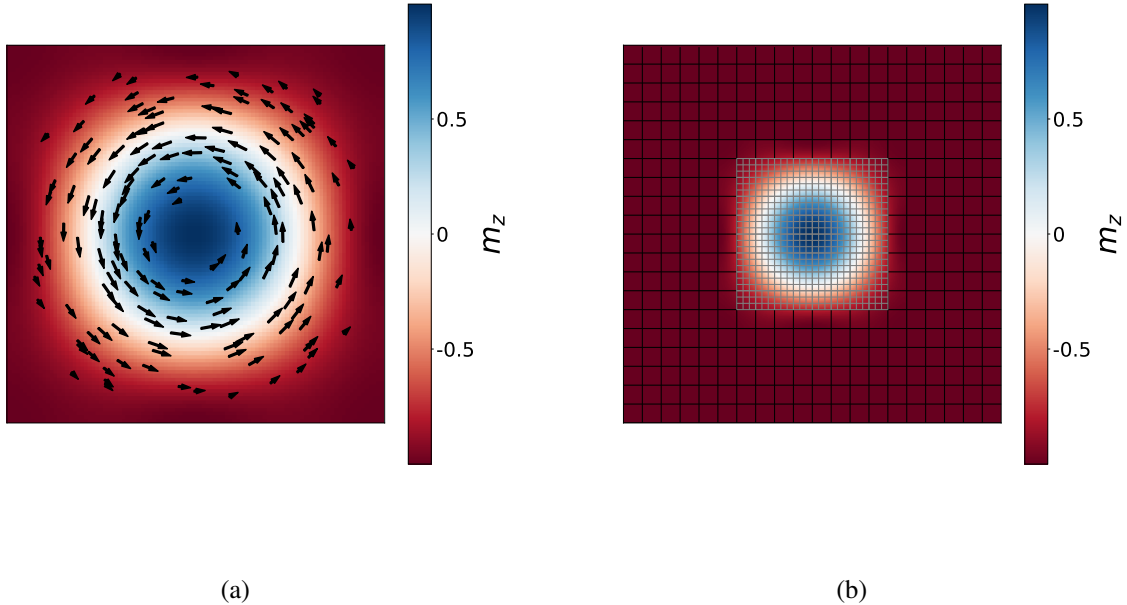


FIG. 1. (a) Illustration of a Bloch skyrmion configuration computed using the micromagnetic model (the pure HB and the multiscale models produce very similar results). The arrows and their size indicate the direction and strength of the in-plane component, the colour indicates the out-of-plane magnetization component. The skyrmion core (blue) is pointing into the plane, whereas the surroundings point out of the plane. In the remainder of this work, we will study such Bloch skyrmions confined in a cylindrical disk-like geometry. The size of a typical skyrmion can reach from a few nanometers up to a few micrometers. (b) The concept of the multiscale approach [25]: A part of the simulation (here shown with the gray mesh) can be computed atomistically, whereas all other parts are computed using the micromagnetic model. A typical application is to use an atomistic region (such as here the skyrmion) for the part of the sample that shows high spin canting and in which the micromagnetic assumption may break down, and use a micromagnetic model for those parts of the sample where the magnetization gradient is lower (such as the nearly homogeneous magnetization surrounding the skyrmion in this pedagogical example).

$$E_{\text{Anisotropy}} = -\mu_0 \sum_i K_u \cdot (\mathbf{S}_i \cdot \mathbf{e}_u)^2 \quad (6)$$

with \mathbf{H}_{ext} the external field, K_u the anisotropy constant and \mathbf{e}_u the unit vector in direction of the low energy axis. The MM expression can be obtained by substituting \mathbf{S} with the MM magnetization vector \mathbf{M} .

The dipolar energy relates to the stray field and can be computed as the sum over all dipole-dipole interactions between two spins. The energy contribution of a magnetic dipole μ_2 exposed

to the stray field H_{μ_1} of dipole μ_1 in the Heisenberg model is

$$E_{\text{Zeeman}} = -\mu_2 \cdot \mathbf{H}_{\mu_1} = \frac{\mu_0}{4\pi} \left(\frac{\mu_1 \cdot \mu_2}{r^3} - 3 \frac{(\mathbf{r} \cdot \mu_1)(\mathbf{r} \cdot \mu_2)}{r^5} \right). \quad (7)$$

with \mathbf{r} the distance of the evaluated spin pair.

The computational effort of the total energy of the system is of complexity $\mathcal{O}(N^2)$ with N being the number of spins, due to its pair-wise nature. For the micromagnetic model, the structure and computational complexity of the equation is for conventional calculations similar and N represents the number of the discretization cells.

A more efficient way of solving this convolution operation is to carry it out in Fourier space [29]. Both the MM and the HB model use a demagnetization tensor combined with a fast Fourier transform (FFT) to calculate the stray field efficiently. While the MM framework uses the demagnetization tensor according to the calculations by Newell et al. [30], the demagnetization tensor $\underline{N}_{\text{HB}}$ of the HB model is calculated as [25]

$$\underline{N}_{\text{HB}} = \frac{1}{4\pi} \left[\frac{\mathbb{1}}{|\mathbf{r}_i - \mathbf{r}_j|^3} - 3 \frac{(\mathbf{r}_i - \mathbf{r}_j) \otimes (\mathbf{r}_i - \mathbf{r}_j)}{|\mathbf{r}_i - \mathbf{r}_j|^5} \right] \quad (8)$$

For the MM simulations the GPU-enabled software package MicroMagnum [31, 32] is used, with extensions for DMI [33]. The HB code is adapted from MicroMagnum, validated in Ref. [25] and was recently parallelized for GPU [34].

D. Multiscale model

To combine the advantages of the micromagnetic (MM) and Heisenberg (HB) simulation models, a multiscale (MS) approach of MicroMagnum is used [25, 34] with DMI included. The central idea is to use a micromagnetic model where possible, and to use the – more accurate and computationally more expensive – HB model where necessary. A schematic sketch of the idea is shown in Fig. 1(b). The MS simulation approach is an efficient method to simulate next generation devices, since large mesoscopic samples have to be simulated micro-magnetically, while HB model accuracy may be necessary for accurate dynamics of the system on atomistic length scales. Both solvers are connected with cross-scale effective field terms for the nearest neighbor interactions as well as for the stray field, which yield a correct transition of the two solver regions. For more details about the embedding and verification of the HB solver into the MM mesh and the time

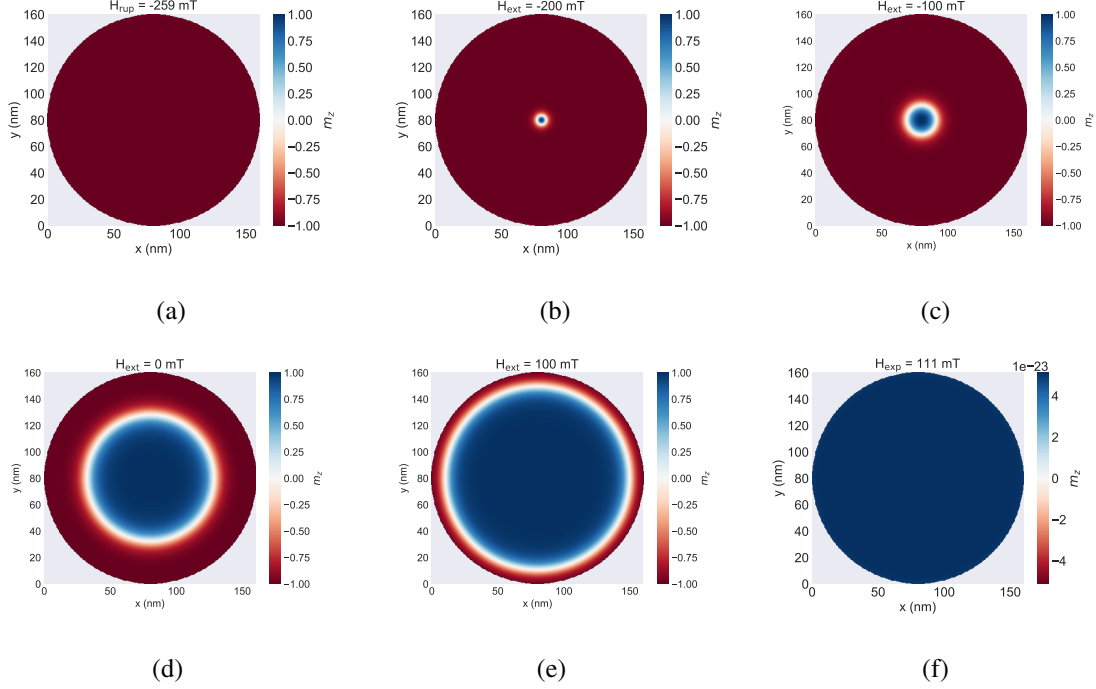


FIG. 2. The process of rupture and expulsion of a skyrmion, starting at zero field (d). Applying the field against the skyrmion core (b,c), its center shrinks until a BP ruptures the topological charge (process is visualized in Fig. 6(a)) and the system stays in the uniform state (a). Applying the field in skyrmion-core direction, it blows up (e) until the topological charge is eliminated at the sample boundaries, also ending up in a uniform state (f). Once the skyrmion is annihilated, it is not possible to reverse the process with an applied field alone.

integration, the reader is referred to Ref. [25]. Our investigation will show in which cases of the skyrmion annihilation a MM simulation is suitable, and when a more accurate HB model is necessary.

E. Torque minimisation

Our expanded MicroMagnum software package (as outlined above) performs micromagnetic and HB simulations on a rectilinear spatial grid. For the relaxation of initial states and determination of (meta-) stable configurations, we use the dissipative Landau-Lifshitz-Gilbert (dLLG) equation [35] to find the steepest gradient energy path, which is given by only the dissipative term of the Landau-Lifshitz equation:

$$\frac{d\mathbf{m}}{dt} = -\alpha\gamma\mathbf{m} \times \mathbf{m} \times \mathbf{H}^{\text{eff}} \quad (9)$$

where \mathbf{m} refers to our (macro-)spin in the respective simulation model (*i.e.* in the Heisenberg model it is the atomistic magnetic moment with $\mathbf{m}\mu = \mathbf{S}$, and in the micromagnetic model the magnetic moment associated with a uniformly magnetized micromagnetic discretisation cell, with $\mathbf{m} \cdot M_S = \mathbf{M}$), α is the damping constant, γ the gyromagnetic ratio, \mathbf{H}^{eff} the effective field acting on the spin, containing all energy contributions. Neglecting the precession term in the Landau-Lifshitz-Gilbert equation is possible here, since we are not interested in the correct precessional dynamics, but only in the relaxed state, *i.e.* we use the dissipative equation to minimize the system's energy. The damping constant is chosen to be $\alpha = 0.5$ to accelerate the process of finding the nearest (meta-)stable configuration.

III. SIMULATION PROTOCOL

The investigated system is a circular disk with diameter $d = 160$ nm and thickness $t = 4.8$ nm. The lattice constant a of the Heisenberg (HB) model is chosen as $a = 0.4$ nm in each direction. For the micromagnetic regions in the multiscale (MS) approach, the cell size was chosen as $\Delta x = \Delta y = 2$ nm, the cell size in z -direction is as thick as the sample: $\Delta z = t = 4.8$ nm, which is a size comparable to the effective thickness of thin-film-systems [13]. The circular shape of the disk is chosen to address the shape of the skyrmion and avoid deformations due to the geometry. We use interfacial DMI, as it is present in thin-film systems with broken inversion symmetry [36].

To determine the skyrmion states, simulations were performed with the following protocol: A skyrmion was artificially put into the system by initializing a uniform state pointing in the z -direction out of the plane with a centered, circular area magnetized in the opposite direction. The radius of this area is chosen with 40 nm. Then this initial state was relaxed to ensure to have at least a skyrmion state as a (meta-)stable state for different values of the material parameters M_S , A , D , and K_u . The relaxation occurs via torque minimization by time integration of the dissipative LLG equation. Fig. 2(d) shows such a configuration, and Sec. IV A and Fig. 3 discusses the observed initial configurations systematically.

Those parameter combinations that exhibit a skyrmion after energy minimization were used for further investigations: we apply out-of-plane fields until the skyrmion is annihilated at an annihilation field H^* , which we aim to determine.

In more detail, the annihilation field H^* was determined by applying an external magnetic out-of-plane (OOP) field either in the direction of the skyrmion core magnetization, or in the opposite

direction to the skyrmion core magnetization.

The field is increased in steps with adjustable step size and a subsequent relaxation, *i.e.* energy minimization. The simulation starts with large field steps. When the skyrmion annihilates, the last stable skyrmion configuration is re-loaded and the field step is then decreased. The process is repeated consecutively with smaller field steps until the desired accuracy of 1 mT in the applied field is reached. More precisely, the field steps are adjusted logarithmically (1000 mT, 100 mT, 10 mT, 1 mT). It is important to not choose too large instantaneous jumps of the field, otherwise an overshooting of the skyrmion during the shrinking process can annihilate it prematurely due to the excited dynamics [37].

For the multiscale model (MS) approach, the simulation was started with just one micromagnetic (MM) region. The Heisenberg (HB) solver is added to the simulation, when the skyrmion is small enough to fit into the 40 nm · 40 nm area, which is the size of the HB solver in the MM simulation. For more details about the implementation and validation of the MS approach we refer to Ref. [25]. Purely HB model and purely MM simulations are performed in the same way for validating and comparison, respectively.

In the case of the applied field acting in the direction of the skyrmion core, we observe an expansion of the skyrmion core, and an unwinding of the magnetization helix at the open boundary of the sample. In this scenario, we call the annihilation field the *expulsion* field $H_{\text{exp}} = H^*$. The process can be seen in subplots 2(d) to 2(f), and is discussed in detail in Sec. IV D. In the expulsion case, we fixed the field step directly at 1 mT, since the relaxation of the increasing skyrmion at larger steps takes more computation time than a larger number of relaxation at smaller field steps.

In the case of the applied field acting in the direction opposite to the magnetization in the skyrmion core, we observe shrinking of the skyrmion core until the skyrmion disappears. In this scenario, we call the annihilation field the *rupture* field $H_{\text{rup}} = H^*$. The process can be seen in subplots 2(d) to 2(a), and is discussed in detail in Sec. IV B.

Regarding the computational models, we run simulations using the micromagnetic model (as it is the fastest), or the multiscale model if required. We have carried out regular simulations with the full HB model (with the assumption that this provides the most accurate numerical solution) to ensure the results of the other computational models are accurate.

While discussed in more detail in the following sections, we summarize key findings already here to guide the reader: the expulsion process can be accurately simulated using the micromagnetic model. For the rupture process, the skyrmion shrinks and collapses when it reaches H_{rup} . At

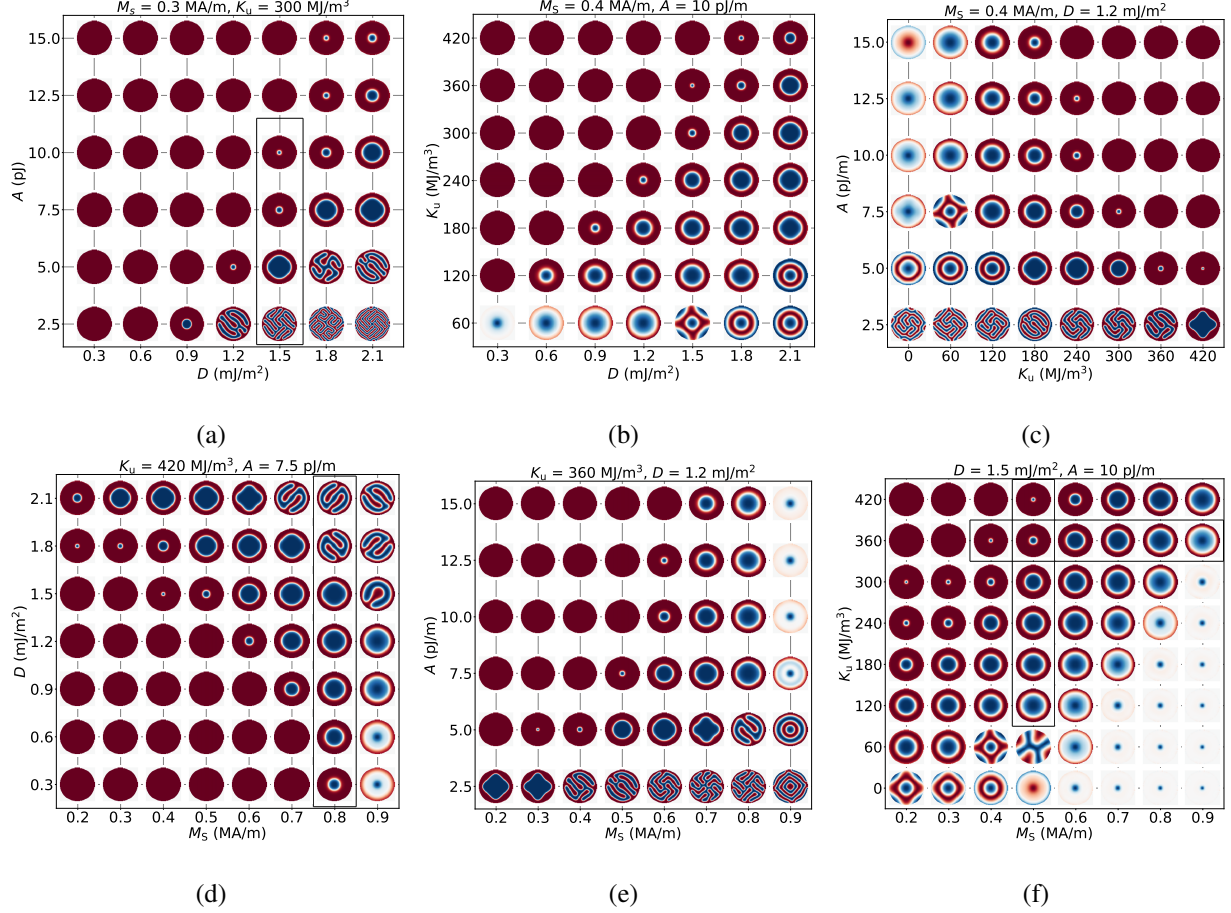


FIG. 3. Meta-stable configurations at zero field for selected magnetic material parameter combinations. Colors indicate the normalized out-of-plane magnetization component (blue = -1, red = 1, white = 0). Six 2D cuts through the phase space are shown. The configuration in each circles show the meta-stable states after relaxation of an initial skyrmion on the 160 nm disk. Configurations enclosed by a black box indicate configuration sets which are analyzed in more detail in the next sections.

that point, the simulation grid is not able to resolve the skyrmion size anymore. We have found that this process needs to be resolved atomistically (Sec. IV C), so that we need to use the multiscale model with an Heisenberg model around the collapsing skyrmion (or use the – computationally more expensive – Heisenberg model for the whole sample).

IV. RESULTS

A. Initial configuration

We follow the procedure described in Sec. III to establish an initial magnetic configuration for each combination of four material parameters. We vary the materials parameter such as the saturation magnetization M_s , anisotropy strength K_u , exchange coupling A and DMI strength D systematically.

Fig. 3 shows such initial configurations obtained for selected parameter combinations. For all of them, there was no external field applied, and they have been calculated in a micromagnetic model with a discretization cell with edge lengths of 2 nm in x and 2 nm in y direction (the two lateral dimensions) and one cell in z direction with edge length $\Delta_z = t = 4.8$ nm. A finer discretization of the disk in the z -direction may change the configuration [38], but we have repeated several data points using the full Heisenberg model, and all reported states are also meta-stable in the Heisenberg model.

We observe different classes of configurations in Fig. 3, including a skyrmion (for example the middle row in Fig. 3(b) for $D \geq 1.2 \text{ mJ/m}^2$), a uniform state (for example left row in Fig. 3(b) for $K_u \geq 120 \text{ MJ/m}^3$), target like configurations in the bottom-right corner of Fig. 3(b), that have also been reported in [38]. Also deformed topological objects are visible, for example in the top-right corner of Fig. 3(d), which carry a topological charge of 1, but do not show a circular shape after the initialization. Fig. 3(e) the three top configurations in the right corner are so called incomplete skyrmions with a topological charge below 1 [38]. We also see two states which undergo a BP reversal, that is resulting from zero anisotropy (for example in Fig 3(c) the top-left configuration). Further, spin spiral states are visible (bottom right corner of Fig. 3(a)).

It is visible from Fig. 3(a), that skyrmions exist within a certain range of the DMI strength D and the exchange constant A . For large values of D , the system relaxes into a spin spiral state, whereas large values of A favor the uniform state (US). Thus, neglecting other effects, skyrmions exist for a distinct ratio A/D . Due to similar effects of A and K_u , the skyrmion states show a band shape in the respective plot, where both values cannot be too high or low, see Fig. 3(c). However, low exchange prefers spin spiral states, while low anisotropy favors target-like states, as visible in Fig. 3(b), 3(c) and 3(f). These findings about the skyrmionic phase are in good agreement with literature [20, 38, 39], where skyrmions are at least meta-stable, when the magnetic parameter configuration

does not differ from the ratio of D/D_c to a great extent, with the critical DMI $D_c = \sqrt{AK}/\pi$. Since we have OOP anisotropy, the effect of increasing K_u is similar to increasing the exchange (Fig. 3(b)). Varying M_S , one sees a transition from the uniform to the skyrmion phase and then into an in-plane configuration above the spin reorientation transition ((d), (e), (f)) [40]. This happens due to the strong far field, which is generated by the OOP magnetization. Lower anisotropy makes the in-plane (IP) skyrmion domain wall (DW) energetically more favorable and can stabilize them in a low K_u and low M_S system (Fig. 3(f)), for $M_S = 0.7 MA/m$. The DW width increases with lower K_u) by reducing surface charges. In an intermediate range of dipolar interactions skyrmions can occur due to stray field stabilization, reducing the far field of the sample. This result is also in agreement with literature [20, 41].

B. Rupture field of skyrmions

Starting from the initial skyrmion states obtained at zero applied field (see Sec. IV A), we now investigate the process of annihilating the skyrmion by applying an external field. In particular, given the initial skyrmion configuration as represented in Fig. 2(d), we apply an external field in the negative z-direction. The skyrmion core will shrink (Fig. 2(c)) in response to this to reduce the Zeeman energy in the core area (where the applied field points in the opposite direction to the magnetization field in the core). As the field is increased further, the skyrmion shrinks further (Fig. 2(b)) and at some point disappears, leading to the configuration shown in Fig. 2(a).

Fig. 4 shows the annihilation process in more detail. We show a cross section side view of the disk, focused at the skyrmion core in the configuration where the skyrmion core has shrunk to its smallest possible size. This is a the situation between Fig. 2(b) and Fig. 2(a). The blue vertical region in Fig. 4(a) is the skyrmion core, and the color represents the z-component of the magnetization, which is pointing in the +z direction in the skyrmion core. The external field is acting in the opposite direction (-z).

These simulation results have been obtained using the Heisenberg model with a 0.4 nm spacing between magnetic moments. As the thickness of the sample is 4.8 nm, we have 12 discrete layers in the z-direction in the HB model. The numbers on the y-axis of the subplots correspond to these layers.

The subplots Fig. 4 (a) to (i) represent different times in the magnetization dynamics that is computed for the annihilation of the skyrmion. We can see in figure (d), (e) and (f) a reversal of

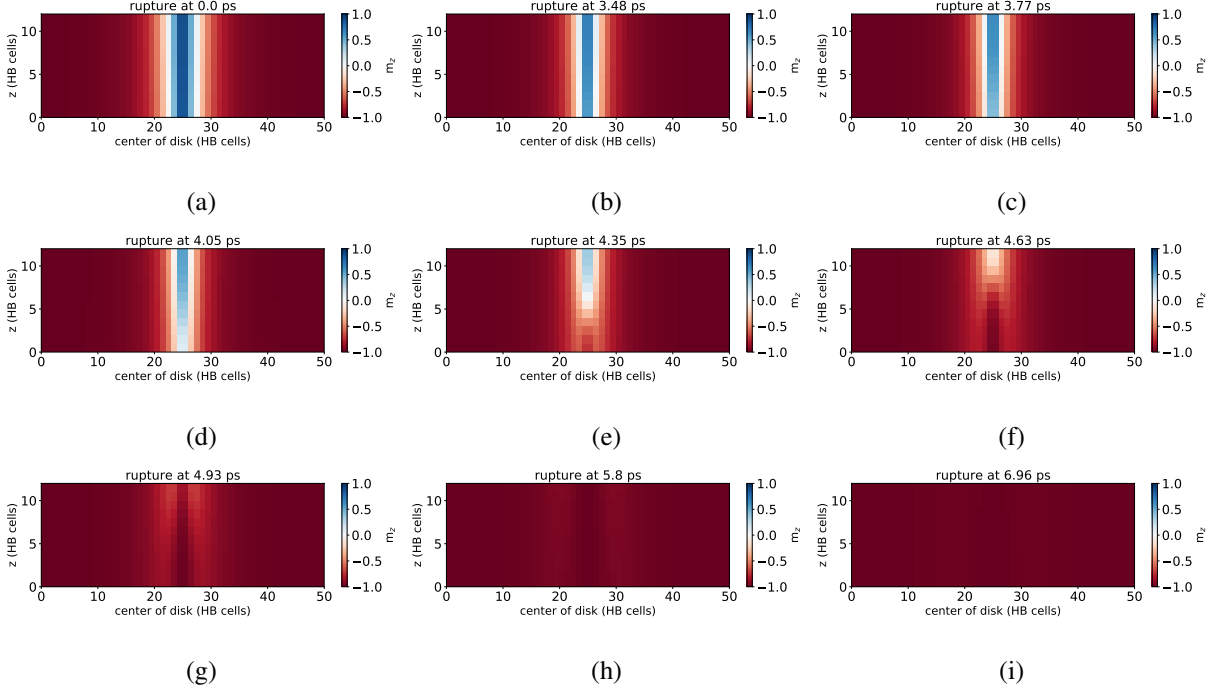


FIG. 4. The rupture process in detail in a side view of the disk: The skyrmion core, as visible in (a), switches its directions in the order of femtoseconds, generating a Bloch point, that travels through the sample (d)-(f) to enable the skyrmion core reversal. The previous skyrmion domain wall still exists after the reversal and the system then transforms into the uniform state. The simulation is counted from a point in time shortly before the reversal occurs.

the magnetization starting from the bottom and propagating towards the top of the sample. The reversal of the skyrmion core is completed in subplot (i).

We interpret the data in subplots (d) to (f) as a Bloch point [24] entering the sample at the bottom and moving up along the skyrmion core to the top of the sample thereby facilitating the reversal [38] of the magnetization. From a topological perspective – where we assume the magnetization vector field is continuous – the skyrmion can only disappear from the sample by breaking that continuity, i.e. by creating a (topological) rupture in the field. This is the reason for describing this annihilation process as the rupture, and the associated applied field at which this annihilation occurs as the *rupture field* H_{rup} and also highlights the importance of the MS model, since these dynamics cannot be resolved in the MM model. For non-skyrmion configurations, we define H_{rup} as the field where the magnetization makes its transition to the uniformly magnetized phase.

We compute this rupture field systematically for those material parameter combinations shown in Fig. 3, following the iterative incrementing of the applied field as described in III.

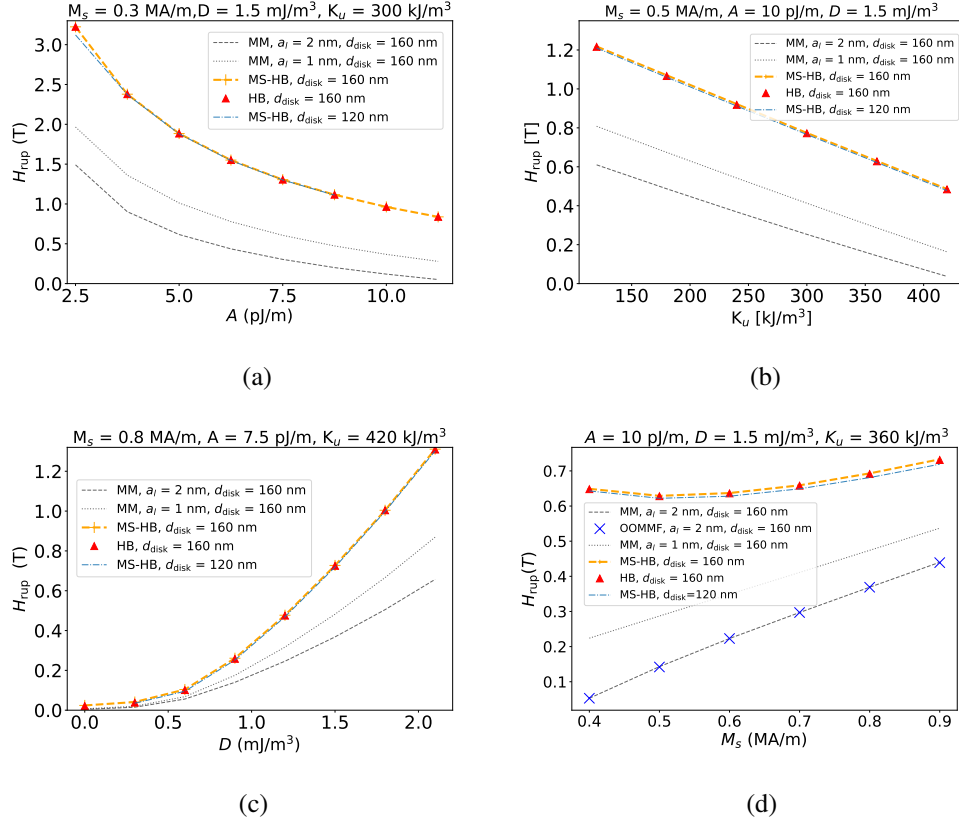


FIG. 5. The rupture field H_{rup} as a function of different magnetic parameters, studied with different computational models, for two geometries. The most important data points are from the Heisenberg (HB) model (red) and the multiscale with Heisenberg (MS) region (yellow). We consider the HB data to be the most accurate data, and the MS data as a computationally efficient approximation. The two data sets are practically identical, and we describe them first, then comment on the other lines shown in addition.

Subplot (a): the rupture field H_{rup} decreases with increasing exchange stiffness A , (b): H_{rup} decreases linearly with the anisotropy constant K_u , (c): H_{rup} increases as a function of DMI strength D , and (d): H_{rup} as a function of saturation magnetization M_s is roughly constant up to $M_s = 0.6 \text{ MA/m}$ and then increases for larger M_s .

The two black lines show results computed using the micromagnetic (MM) model (black) for a discretisation cell size of 1 nm (dotted) and 2 nm (dashed). The micromagnetic model results should be independent of the chosen discretization length: as this is not the case, the main observation is that the micromagnetic model does not accurately describe the rupture process.

The blue crosses in plot (d) show results computed with OOMMF. This is evidence that our micromagnetic model agrees with the OOMMF micromagnetic model as benchmark.

All of the data discussed above is for a disk diameter of 160 nm. In addition, the thin blue line shows multiscale model results for a diameter of 120 nm, to give an indication of the sensitivity of H_{rup} to the geometry.

Fig. 5 shows the rupture field as a function of one material parameter per subfigure for a subset of all combinations. Fig. 9 in the appendix shows the rupture field for all the configurations shown in Figure 3.

Fig. 5(a) shows the rupture field H_{rup} as a function of exchange stiffness A , where H_{rup} decreases with increasing A . A strong exchange constant A favors the uniform configuration, since the exchange energy is minimized for a parallel alignment of the spins in a ferromagnet. We can also look at the energy of a (skyrmion) domain wall for which the energy density is given by [42]:

$$\sigma_{DW} \propto 4\sqrt{AK} - \pi|D| \quad (10)$$

The energy of the skyrmion will thus increase for increasing A mainly due to the spin canting in the DW. Thus, the presence of DWs becomes energetically unfavorable with increasing A , increasing the energy level for the skyrmion and in this case consequently lowering the energy barrier towards the uniform configuration.

Fig. 5(b) shows that the rupture field decreases (linearly) with increasing values of the anisotropy strength K_u . For small K_u one is closer to the spin reorientation transition, this stabilizes the skyrmion DW, since in-plane configurations are more favorable compared to systems with high anisotropy, leading to a lower energy of the skyrmion state in comparison to the uniformly magnetized configuration. The energy of the FM state decreases since the absolute value of E_{ani} decreases with increasing anisotropy strength. A similar linearity is also given in the simpler Stoner-Wolfarth (SW) model [43]. The model describes a hysteretic behavior of single-domain ferromagnets, while the coercive field H_C of the systems scales linearly with the anisotropy constant, $H_C = 2 \cdot K/M_S$. The coercive field in the SW model is the field strength at which a sample shows zero net magnetization. While H_C increases with K , we see a linear decrease of H_{rup} with the anisotropy.

Fig. 5(c) shows the DMI strength dependence of H_{rup} , which increases for higher D . The DMI stabilizes chiral spin structures and favors the skyrmion state compared to the FM state. The energy of the skyrmion state shrinks, resulting in a higher energy barrier, assuming a scaling of the barrier between the FM and the skyrmion state. The energy of the FM state should increase with higher D since the parallel alignment does not minimize E_{DMI} . Results are thus in agreement with previous publications [12, 37] for the skyrmion rupture. H_{rup} increases with D in the whole range of (meta-)stable skyrmions.

Fig. 5(d) shows data for the influence of M_S on the annihilation field. Due to stronger dipolar

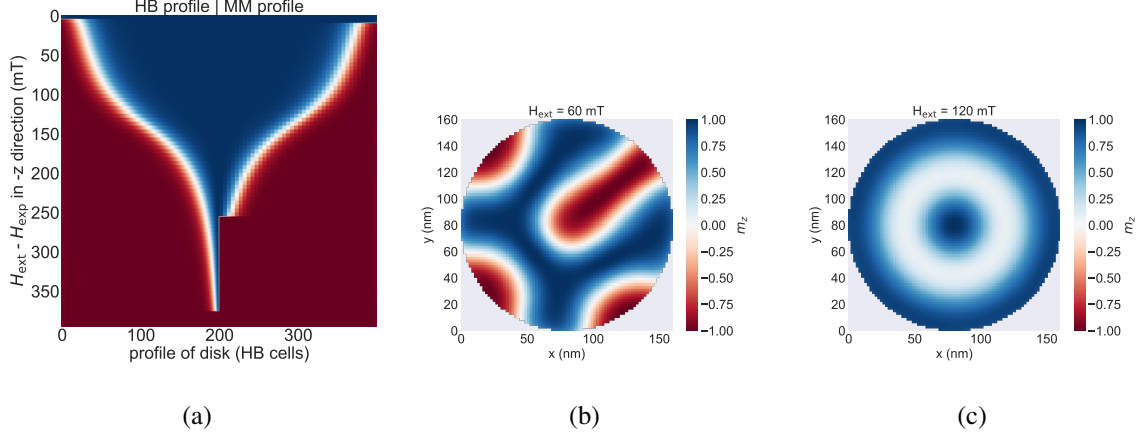


FIG. 6. (a) Dependence of the skyrmion profile on the field and the computational model. The x-axis represents a line scan through the disk in the diametric direction with the skyrmion core at the center (at position 200). The color shows the z-component of the magnetization. The left side of the plot (up to HB cell 200) is taken from a Heisenberg model (with an lateral magnetic moment spacing of 0.4 nm), whereas the right (HB cell 201 and larger) is taken from the micromagnetic model calculations with 2 nm lateral cell size. (b) Transition state during the expulsion of the simulation point in Fig. 7(b), for $K_u = 120 \text{ MJ/m}^3$. The skyrmion is not directly expelled, but undergoes a transition into a spin spiral state. (c) Transition state during the expulsion of the simulation point in Fig. 7(d), for $M_S = 0.9 \text{ MA/m}$. The skyrmion is not directly expelled, but undergoes a transition into a target configuration without a negative components.

interactions between the skyrmion core and the ring with opposite magnetization surrounding the skyrmion, higher M_S stabilizes the skyrmion. A stronger stray field should increase the energy of the FM state due to the stronger far field of this configuration. The combined effect can lead to an increasing H_{rup} for larger M_S .

We repeat the simulations for a smaller disk size ($d_{\text{disk}} = 120 \text{ nm}$ instead of $d_{\text{disk}} = 160 \text{ nm}$). The resulting data for the rupture field is also displayed in each subplot of Fig. 5. The qualitative behavior is the same as for the disk with $d_{\text{disk}} = 160 \text{ nm}$. Quantitatively, the values are up to a few percent lower. Those changes are small, although the area of the disk decreased by nearly a half, reducing, for example, the stabilizing stray field. Our interpretation is that the annihilation of the small skyrmion is the dominating factor in the process. For this, it does not matter much how large the disk is.

C. Limit of the micromagnetic model

In Fig. 5 the dependence of the annihilation field H_{rup} on single magnetic parameters is shown in more detail. To underline the importance of the simulation model, we performed the described simulations above in a purely micromagnetic model with different lateral cell sizes ($a_1 = 2$ nm and $a_1 = 1$ nm), and also in a full Heisenberg model, and using the multiscale model (see Sec. II).

The data based based on the micromagnetic (MM) model in Fig. 5 deviate very substantially from the HB model results. This shows that MM simulations with the chosen cell size (which is typical for micromagnetic studies) can lead to inaccurate results.

We have repeated the micromagnetic simulations carried out using MicroMagnum with the Object-Oriented MicroMagnetic Framework (OOMMF) [44] which was driven through the uber-mag framework [45]. One set of results is shown in Fig. 5(d) and agrees with the results obtained using MicroMagnum. This is evidence that the observed deviation between Heisenberg and micromagnetic model originates from the micromagnetic model rather than our MicroMagnum implementation of it.

We conclude that very small skyrmions, as they occur in the annihilation process based on the shrinking of the skyrmion, cannot be resolved in a coarse mesh as used for micromagnetics anymore. Fig. 6(a) shows the skyrmion size in the HB (on the left) and the MM model (on the right) within the same subplot. The x-axis represents a spatial coordinate of a scan through the disk, where for position < 200 data from the Heisenberg model is used, and for the position > 200 data from the micromagnetic model is used. The y-axis correlates to the changing external field. The width of the blue region in the x-direction corresponds to the size of the skyrmion core. We see in Fig. 6(a) that the skyrmion size is in both models very similar, as long as the MM model is able to host the skyrmion. The pure HB model gives the most accurate result, and is able to resolve a much smaller skyrmion (on the left) than the micromagnetic model (on the right) can do. It is therefore not surprising that the micromagnetic description of the annihilation process – that involves the shrinking and then annihilation of the skyrmion via a topological rupture – depends strongly on the chosen discretisation when computed with the micromagnetic model, and is thus inaccurate. Alternative computational models include the HB model, which is computationally too expensive. The multiscale model, which combines the Heisenberg model and the micromagnetic model, is a compromise that provides good accuracy where necessary and good performance through use of the micromagnetic model where possible.

In Fig. 5 we compare results computed using the multiscale (MS) model and the Heisenberg model (HB). We find that the multiscale model over-estimates the rupture field by only 1-2 mT, which is just above the chosen field step size of 1 mT. The small overestimation might come from the overestimation of the stray field due to the exclusive MM part of the sample: since there is no discretization in z-direction, the stray field might be higher than in a calculation performed in the full HB model, where spins can tilt at the surface due to demagnetization effects. However, the MS approach is not limited to any discretization of the MM mesh, also allowing for discretization in z-direction. The chosen discretization however shows sufficient accuracy for our purpose. Thus, the MS approach can provide a fast and robust evaluation of spin dynamics in larger samples, where HB calculations are not feasible.

We also want to discuss briefly the effect of temperature on the simulation results. In general, thermal noise should lower the annihilation fields, since the random fluctuations allow the system to reach energetically higher states. However, increasing the temperature of a sample can also vary the magnetic parameters drastically [46]. We expect this effect to have a much higher influence on the annihilation field, since varying those parameters may change H_{rup} by some factors, as can be seen in Fig. 5. While the HB model is able to simulate temperature effects accurately, the MM model has only restricted possibilities to simulate those effects, since the cell discretization leads to a cut-off of the spin wave spectrum at wavelengths in the order of the cell size. It might be challenging to include thermal effects in the multiscale model, since the wave spectra at the interface need to be treated in a way that minimize errors in the cross-scale embedding.

D. Expulsion field of skyrmions

Starting from the initial skyrmion states obtained at zero applied field (see Sec. IV A), we now investigate the process of annihilating the skyrmion by applying an external field in the positive z-direction. (Section IV B discusses the application of the field in the negative z-direction.)

In the context of the initial skyrmion configuration as represented in Fig. 2(d), we apply the external field in the positive z-direction, which is the direction of the skyrmion core. The core will grow in response to the applied field because this will reduce the Zeeman energy of the system. When the skyrmion core has expanded so far that the skyrmion's helix approaches the disk's boundary, the magnetization helix can unwind at the boundary (without rupturing the continuous magnetization vector field).

Subplots 2(d) to 2(f) show the process of expulsion. In this scenario, we call the annihilation field the *expulsion* field $H_{\text{exp}} = H^*$.

We define H_{exp} as the lowest field value, at which no magnetization component is pointing against the field direction, which means when $\min(m_z) \geq 0$. During simulation of the field application, some of the intermediate magnetic configurations may not be skyrmion configurations but more complex spin spiral structures.

Fig. 7 shows the dependence of H_{exp} on different magnetic parameters. In contrast to the application of the field in the opposite direction – and the associated skyrmion annihilation through skyrmion shrinking and rupture, the expulsion process is within the domain of applicability of the micromagnetic model, and thus the Heisenberg and the micromagnetic model provide very comparable results (and there is no need to use the multiscale model). We will discuss here the results of the micromagnetic approach. Fig. 7(a) shows the dependence of the expulsion field as a function of the exchange coupling. Similar as for the rupture process in Fig. 5(a), a strong exchange lowers H_{exp} as the uniform configuration becomes energetically more attractive than the skyrmion with increasing exchange coupling. Although the skyrmion radius is smaller for a stronger exchange constant A at zero-field (see for example Fig. 3(a)), the skyrmion increases in size much faster with increasing field, leading to an expulsion at the disk boundary at lower fields. In Fig. 7(b) an approximately linear dependence of H_{exp} for K_u is observed over a wide range of anisotropy strengths. A strong anisotropy avoids large IP components and thus tries to prevent the IP skyrmion DW for strong size increase with increased field strengths. Such linear behavior was also observed for H_{rup} . However, one outlier for $K_u = 120 \text{ MJ}/\text{m}^3$ is observed. This configuration has a transition into a spin spiral states during the field ramping, which leads to the discontinuous behavior. The configuration is also shown in Fig. 6(b).

As seen in Fig. 7(c), for the DMI we find an increase in H_{exp} for stronger D , similar as for the rupture. A skyrmion configuration reduces the DMI energy in the system with high D , on the same hand the energy of the FM state increases, also increasing the barrier between the states. For strong DMI, H_{exp} therefore is higher.

As visible in Fig. 7(d), the dependence of H_{exp} on M_S shows a dip for intermediate values, rising slowly again for $M_S = 0.8 \text{ MA}/\text{m}$. For this value the system is close to the spin reorientation transition, when the system loses perpendicular magnetic anisotropy and favors IP magnetization. In Fig. 7(d), a special case is the point for 160 nm disk size and $M_S = 0.9 \text{ MA}/\text{m}$. Here, a target configuration evolves without negative z-component, see Fig. 6(c), reaching the criteria for the

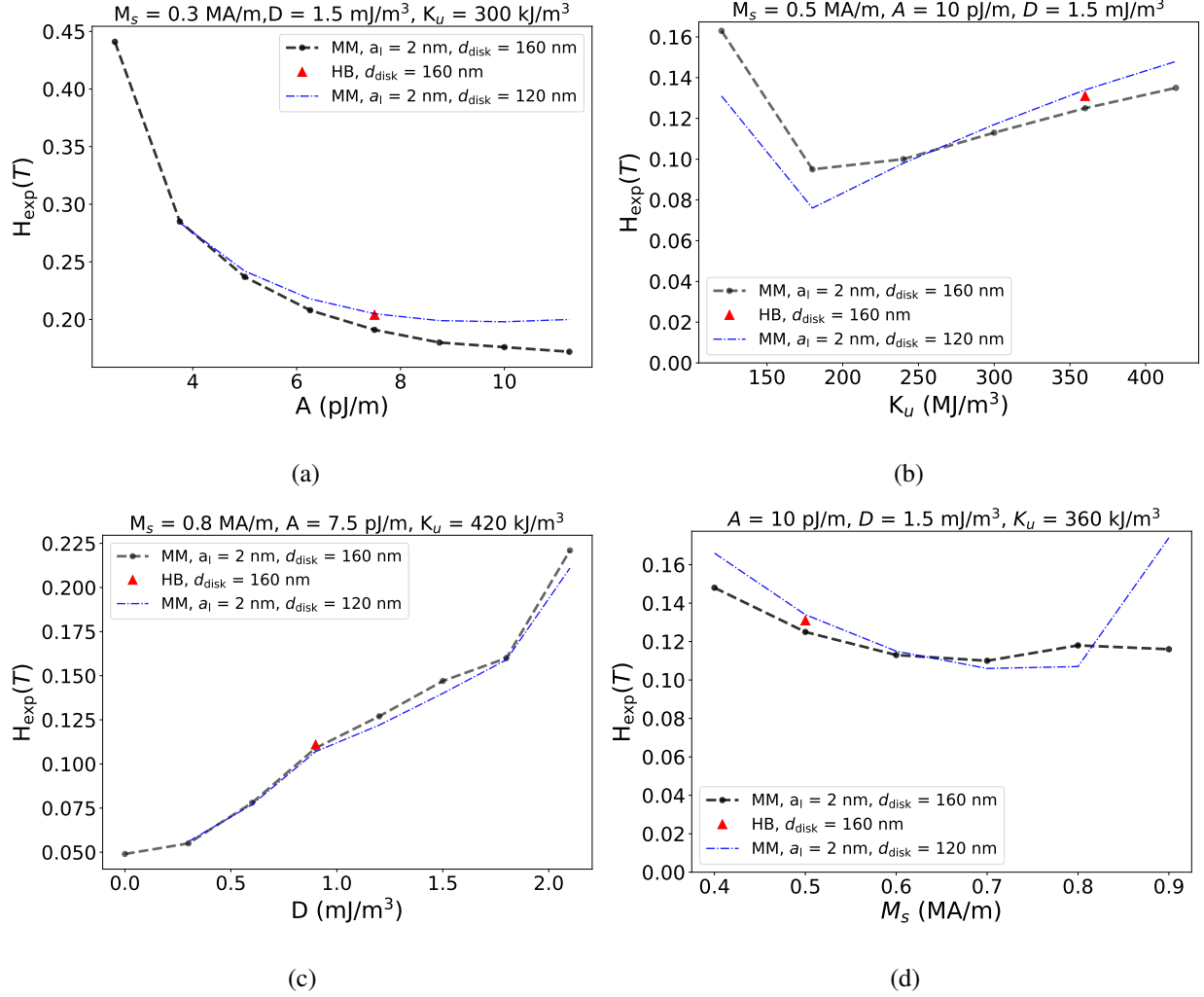


FIG. 7. The expulsion field H_{exp} as a function of different magnetic parameters. HB, multiscale and micromagnetic simulations are in very good agreement for the data shown here, and only the micromagnetic data is shown. Grey lines indicate the transition into non-skyrmionic states for the usual disk diameter. The dependence of the expulsion field H_{exp} is shown as a function of (a) exchange stiffness A , (b) anisotropy constant K_u , (c) DMI strength D , and (d) saturation magnetization M_s .

chosen definition of H_{exp} . For the smaller disk size the qualitative behavior is the same, except for an outlier for large M_s , where the magnetic states transitions into a non-skyrmionic configuration with large IP component.

Changing the disk size affects the expulsion process more strongly than the rupture process. We find a maximum change of around 25% when comparing the expulsion field for the disk with 120 nm to the disk with 160 nm diameter (neglecting the discussed special cases with complex transition states). The expulsion is not a localized process and thus depends strongly on the sample

geometry and the skyrmion size dependence on the field. For different parameter sets, H_{exp} might increase or decrease. Fig. 8 shows two different skyrmion diameters for two parameter sets from Fig. 7(b). Fig. 8(a) shows the case where the smaller disk has a lower H_{exp} , Fig. 8(b) shows the case, where the smaller disk has a higher H_{exp} . The first case shows stray-field stabilized skyrmions also at zero field. Both skyrmions increase their size approximately linearly, while the larger disk size allows for a larger size before the expulsion takes place. In the latter case - DMI-stabilized skyrmions at zero field - we see a large, sudden increase of the skyrmion size at around 50 mT, which is the transition from the DMI-stabilization to a stray-field-stabilization [20]. In that case, the jump is less distinct for the smaller disk, caused by less stray field in a smaller sample. Due to this effect, the relative size of the skyrmion in the stray-field-stabilized regime is smaller for the disk with $d = 120$ nm, and the following linear increase due to the field stabilizes a skyrmion at higher fields than in the large disk. This leads to different trends of H_{exp} by changing disk sizes.

For the expulsion process, there is no need to use a HB model, since no BP or other strong spin canting occurs which would require a more accurate model. Small deviations between the HB and the MM model may originate from discretization errors, since the chosen finite difference method [47] approximates the circular disk by a rectangular mesh.

We also find that for most parameter sets H_{exp} is in general around one order of magnitude smaller than H_{rup} , since the topological charge does not protect the spin structure against expulsion.

V. CONCLUSION

We have investigated the process of the transition from a skyrmion in a disk geometry to a uniformly magnetized state using an external magnetic field that is applied in the out-of-plane direction. We find two different reversal mechanisms, depending on the direction of the applied field relative to the direction of the magnetization in the skyrmion core.

If the direction of the magnetization in the core of the skyrmion points into the same direction as the applied field, then the skyrmion core will grow with an increasing field, until the whole disk is uniformly magnetized in the direction of the applied field. The skyrmion in this expulsion process is driven out of the sample by growing the core, and the skyrmion domain wall unwinding at the circumferential boundary of the disk geometry.

If the direction of the applied field points into the opposite direction of the magnetization in

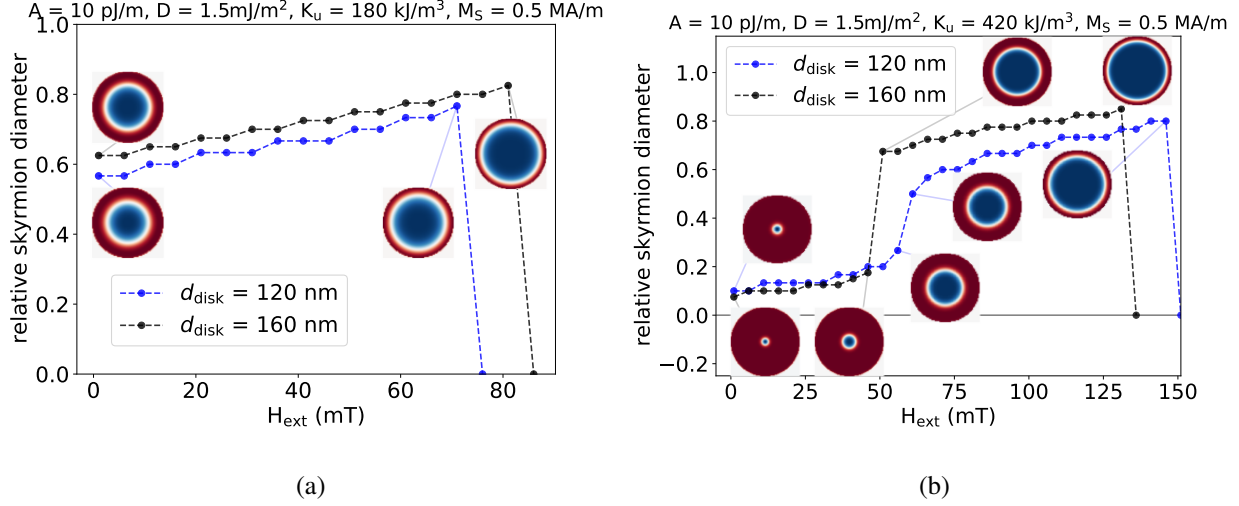


FIG. 8. (a): Skyrmion radius for selected parameter sets from Figure 7(b) for different disk sizes. Insets show the magnetic configuration at the respective field. It is clearly visible that small skyrmions at lower fields show a large step during the transition from DMI-stabilization to strayfield-stabilization (in (b) at around 50 mT). This jump is considerably smaller for smaller disk sizes due to smaller stray fields in that sample, which then results in a higher expulsion field.

the corner, then the skyrmion core shrinks with increasing external field strength, until the field is sufficiently strong to remove the skyrmion from the sample. In the process, a rupture of the magnetization vector field occurs to allow for the skyrmion to be annihilated at the center of the disk. The microscopic annihilation mechanism is facilitated by a Bloch point moving through the thickness of the sample, which reverses the direction of the core.

For both directions, we have determined the required strength of the applied field that is required to annihilate the skyrmion from the sample, and which we refer to as the expulsion field and the rupture field, depending on the mechanism of the annihilation of the skyrmion.

We have shown that the rupture field H_{rup} of skyrmions in a confined geometry depends strongly on the materials parameters, while the dependence on the disk size is rather small in the observed regime of around 100 nm. The independence on the results of the disk size relates to the annihilation of the skyrmion taking place in the centre of the disk as a local process, for which the total size of the disk is not important. The disk size plays a large role for the expulsion process though, as the skyrmion core grows until it reaches the boundary of the disk. We find that the skyrmion expulsion field H_{exp} is in general one order of magnitude smaller than H_{rup} , since no highly energetic BP occurs during the annihilation of the topological charge.

For the potential use of skyrmions in a data storage device, the skyrmion lifetime has to be chosen in way, that on the one hand imprinting a state is possible and energy efficient, but on the other hand data retention has to be ensured over the device lifetime (or at least a reasonable time span) in the presence of thermal fluctuations. The energy barrier, probed indirectly by our investigations, is the main parameter to adjust this trade-off. One important outcome of these investigations is, that it is easier to annihilate the skyrmion state without generating a BP. This result is consistent with other studies where a smaller energy barrier was found for skyrmions to disappear via a sample boundary rather than through shrinking [12].

With skyrmions in confined geometries one could imagine to design a bit-patterned-media (BPM) storage device [15], which is able to store more than one bit in one geometry: at least four states are imaginable as meta-stable states for the disks (skyrmion up, uniform up, skyrmion down, uniform down). This would lead to a potentially very significant increase of the storage capacity for such devices: with n binary storage units (i.e. bits) one can encode 2^n states, whereas with n storage units of this base 4, the number of storable bits doubles for the same amount of bit patterns.

We have used two different simulation models, a Heisenberg model and a micromagnetic model. We have found that the micromagnetic model cannot resolve accurately the annihilation process due to BP formations: The computed behavior depends on the micromagnetic cell size which, however, should not affect the observed physics in a reliable simulation. In the rupture process, the skyrmion core shrinks down to one line of magnetic moments, which cannot be resolved in the micromagnetic representation.

In all other simulations we have found close agreement between the Heisenberg model and the micromagnetic model. Where the micromagnetic model cannot be used but the Heisenberg model is computationally too expensive to employ, a multiscale model has been used successfully which represents the sample in the Heisenberg model where necessary and in the micromagnetic model where possible.

ACKNOWLEDGMENTS

Thomas Winkler and the group in Mainz acknowledge funding from the Emergent AI Center, funded by the Carl-Zeiss-Stiftung, the German Research Foundation (DFG SFB TRB 173,

SPIN+X, A01 403502522; SPP Skyrmionics) and the European Research Council (ERC-2019-SyG, 3D MaGiC, ID: 856538). This work was also financially supported by the Engineering and Physical Sciences Research Council’s UK Skyrmion Project Grant (EP/N032128/1). We further acknowledge for fruitful discussions with Ulrich Nowak, Oleg Tretiakov and Karin Everschor-Sitte.

-
- [1] K. Everschor-Sitte, J. Masell, R. M. Reeve, and M. Kläui, “Perspective: Magnetic skyrmions—overview of recent progress in an active research field,” *Journal of Applied Physics*, vol. 124, no. 24, p. 240901, 2018.
- [2] Y. Tokura and N. Kanazawa, “Magnetic skyrmion materials,” *Chemical Reviews*, vol. 121, no. 5, pp. 2857–2897, 2021. PMID: 33164494.
- [3] I. Dzyaloshinsky, “A thermodynamic theory of “weak” ferromagnetism of antiferromagnetics,” *Journal of Physics and Chemistry of Solids*, vol. 4, no. 4, pp. 241–255, 1958.
- [4] T. Moriya, “Anisotropic superexchange interaction and weak ferromagnetism,” *Phys. Rev.*, vol. 120, pp. 91–98, Oct 1960.
- [5] D. Pinna, F. A. Araujo, J.-V. Kim, V. Cros, D. Querlioz, P. Bessière, J. Droulez, and J. Grollier, “Skyrmion gas manipulation for probabilistic computing,” *Phys. Rev. Applied*, vol. 9, p. 064018, Jun 2018.
- [6] J. Zázvorka, F. Jakobs, D. Heinze, N. Keil, S. Kromin, S. Jaiswal, K. Litzius, G. Jakob, P. Virnau, D. Pinna, *et al.*, “Thermal skyrmion diffusion used in a reshuffler device,” *Nature nanotechnology*, vol. 14, no. 7, pp. 658–661, 2019.
- [7] R. Tomasello, E. Martinez, R. Zivieri, L. Torres, M. Carpentieri, and G. Finocchio, “A strategy for the design of skyrmion racetrack memories,” *Sci. Rep.*, vol. 4, p. 6784, 2014.
- [8] A. Fert, V. Cros, and J. Sampaio, “Skyrmions on the track,” *Nat. Nanotechnol.*, vol. 8, pp. 152–156, 2013.
- [9] F. Büttner, I. Lemesch, M. Schneider, B. Pfau, C. M. Günther, P. Hession, J. Geilhufe, L. Caretta, D. Engel, B. Krüger, *et al.*, “Field-free deterministic ultrafast creation of magnetic skyrmions by spin–orbit torques,” *Nat. Nanotechnol.*, vol. 12, pp. 1040–1044, 2014.
- [10] S. Finizio, K. Zeissler, S. Wintz, S. Mayr, T. Weßels, A. J. Huxtable, G. Burnell, C. H. Marrows, and J. Raabe, “Deterministic field-free skyrmion nucleation at a nanoengineered injector device,” *Nano*

- Letters*, vol. 19, no. 10, pp. 7246–7255, 2019.
- [11] S. Woo, K. M. Song, X. Zhang, M. Ezawa, Y. Zhou, X. Liu, M. Weigand, S. Finizio, J. Raabe, M.-C. Park, *et al.*, “Deterministic creation and deletion of a single magnetic skyrmion observed by direct time-resolved x-ray microscopy,” *Nature Electronics*, vol. 1, no. 5, pp. 288–296, 2018.
- [12] D. Cortés-Ortuño, W. Wang, M. Beg, R. A. Pepper, M.-A. Bisotti, R. Carey, M. Vousden, T. Kluyver, O. Hovorka, and H. Fangohr, “Thermal stability and topological protection of skyrmions in nanotracks,” *Scientific reports*, vol. 7, no. 1, pp. 1–13, 2017.
- [13] S. Woo, K. Litzius, B. Krüger, M.-Y. Im, L. Caretta, K. Richter, M. Mann, A. Krone, R. M. Reeve, M. Weigand, *et al.*, “Observation of room-temperature magnetic skyrmions and their current-driven dynamics in ultrathin metallic ferromagnets,” *Nature Materials*, vol. 15, no. 5, pp. 501–506, 2016.
- [14] K. Litzius, I. Lemesh, B. Krüger, P. Bassirian, L. Caretta, K. Richter, F. Büttner, K. Sato, O. A. Tretiakov, J. Förster, *et al.*, “Skyrmion hall effect revealed by direct time-resolved x-ray microscopy,” *Nature Physics*, vol. 13, no. 2, pp. 170–175, 2017.
- [15] H. Richter, A. Dobin, O. Heinonen, K. Gao, R. vd Veerdonk, R. Lynch, J. Xue, D. Weller, P. Asselin, M. Erden, *et al.*, “Recording on bit-patterned media at densities of 1 tb/in² and beyond,” *IEEE Transactions on Magnetics*, vol. 42, no. 10, pp. 2255–2260, 2006.
- [16] S. H. Charap, P.-L. Lu, and Y. He, “Thermal stability of recorded information at high densities,” *IEEE Transactions on Magnetics*, vol. 33, no. 1, pp. 978–983, 1997.
- [17] K. Litzius, I. Lemesh, B. Krüger, P. Bassirian, L. Caretta, K. Richter, F. Büttner, K. Sato, O. A. Tretiakov, J. Förster, *et al.*, “Skyrmion hall effect revealed by direct time-resolved x-ray microscopy,” *Nature Physics*, vol. 13, no. 2, pp. 170–175, 2017.
- [18] B. Göbel and I. Mertig, “Skyrmion ratchet propagation: utilizing the skyrmion hall effect in ac race-track storage devices,” *Scientific reports*, vol. 11, no. 1, pp. 1–11, 2021.
- [19] J. Zázvorka, F. Dittrich, Y. Ge, N. Kerber, K. Raab, T. Winkler, K. Litzius, M. Veis, P. Virnau, and M. Kläui, “Skyrmion lattice phases in thin film multilayer,” *Advanced Functional Materials*, vol. 30, no. 46, p. 2004037, 2020.
- [20] F. Büttner, I. Lemesh, and G. S. Beach, “Theory of isolated magnetic skyrmions: From fundamentals to room temperature applications,” *Scientific reports*, vol. 8, no. 1, pp. 1–12, 2018.
- [21] L. Desplat, C. Vogler, J.-V. Kim, R. Stamps, and D. Suess, “Path sampling for lifetimes of metastable magnetic skyrmions and direct comparison with kramers’ method,” *Physical Review B*, vol. 101, no. 6, p. 060403, 2020.

- [22] R. Zivieri and O. Chubykalo-Fesenko, “Static properties of magnetic skyrmions,” in *Magnetic Skyrmions and Their Applications*, pp. 181–231, Elsevier, 2021.
- [23] W. F. Brown Jr, “Thermal fluctuations of a single-domain particle,” *Physical review*, vol. 130, no. 5, p. 1677, 1963.
- [24] E. Feldtkeller, “Mikromagnetisch stetige und unstetige magnetisierungskonfigurationen,” *Zeitschrift fur Angewandte Physik*, vol. 19, no. 6, pp. 530–+, 1965.
- [25] A. De Lucia, B. Krüger, O. A. Tretiakov, and M. Kläui, “Multiscale model approach for magnetization dynamics simulations,” *Physical Review B*, vol. 94, no. 18, p. 184415, 2016.
- [26] D. Hinzke and U. Nowak, “Monte carlo simulation of magnetization switching in a heisenberg model for small ferromagnetic particles,” *Computer physics communications*, vol. 121, pp. 334–337, 1999.
- [27] S. Blundell, “Magnetism in condensed matter,” 2003.
- [28] T. Lancaster and S. J. Blundell, *Quantum field theory for the gifted amateur*. OUP Oxford, 2014.
- [29] C. Abert, L. Exl, G. Selke, A. Drews, and T. Schrefl, “Numerical methods for the stray-field calculation: A comparison of recently developed algorithms,” *Journal of Magnetism and Magnetic Materials*, vol. 326, pp. 176–185, 2013.
- [30] A. J. Newell, W. Williams, and D. J. Dunlop, “A generalization of the demagnetizing tensor for nonuniform magnetization,” *Journal of Geophysical Research: Solid Earth*, vol. 98, no. B6, pp. 9551–9555, 1993.
- [31] A. Drews, G. Selke, B. Krueger, *et al.*, “Micromagnum github repository, <https://github.com/micromagnum/micromagnum>,” 2014.
- [32] G. Selke, *Design and Development of a GPU-accelerated Micromagnetic Simulator*. PhD thesis, Staats-und Universitätsbibliothek Hamburg Carl von Ossietzky, 2013.
- [33] K. Litzius, *Spin-orbit-induced Dynamics of Chiral Magnetic Structures: Skyrmion Dynamics in Thin Film Devices at Varying Temperatures*. PhD thesis, Johannes Gutenberg-Universität Mainz, 2018.
- [34] T. Winkler, “Simulation and detection of confined spin structures,” Master’s thesis, Johannes Gutenberg Universität Mainz, 2018.
- [35] A. V. Ivanov, D. Dagbartsson, J. Tranchida, V. M. Uzdin, and H. Jónsson, “Efficient optimization method for finding minimum energy paths of magnetic transitions,” *Journal of Physics: Condensed Matter*, vol. 32, no. 34, p. 345901, 2020.
- [36] S. Emori, U. Bauer, S.-M. Ahn, E. Martinez, and G. S. Beach, “Current-driven dynamics of chiral ferromagnetic domain walls,” *Nature materials*, vol. 12, no. 7, pp. 611–616, 2013.

- [37] A. De Lucia, K. Litzius, B. Krüger, O. A. Tretiakov, and M. Kläui, “Multiscale simulations of topological transformations in magnetic-skyrmion spin structures,” *Physical Review B*, vol. 96, no. 2, p. 020405, 2017.
- [38] M. Beg, R. Carey, W. Wang, D. Cortés-Ortuño, M. Vousden, M.-A. Bisotti, M. Albert, D. Chernyshenko, O. Hovorka, R. L. Stamps, *et al.*, “Ground state search, hysteretic behaviour and reversal mechanism of skyrmionic textures in confined helimagnetic nanostructures,” *Scientific reports*, vol. 5, no. 1, pp. 1–14, 2015.
- [39] W. Akhtar, A. Hrabec, S. Chouaieb, A. Haykal, I. Gross, M. Belmeguenai, M. Gabor, B. Shields, P. Maletinsky, A. Thiaville, *et al.*, “Current-induced nucleation and dynamics of skyrmions in a co-based heusler alloy,” *Physical Review Applied*, vol. 11, no. 3, p. 034066, 2019.
- [40] U. Gradmann and J. Müller, “Flat ferromagnetic, epitaxial 48ni/52fe (111) films of few atomic layers,” *physica status solidi (b)*, vol. 27, no. 1, pp. 313–324, 1968.
- [41] C. Chui, F. Ma, and Y. Zhou, “Geometrical and physical conditions for skyrmion stability in a nanowire,” *AIP Advances*, vol. 5, no. 4, p. 047141, 2015.
- [42] A. Thiaville, S. Rohart, É. Jué, V. Cros, and A. Fert, “Dynamics of dzyaloshinskii domain walls in ultrathin magnetic films,” *EPL (Europhysics Letters)*, vol. 100, no. 5, p. 57002, 2012.
- [43] E. C. Stoner and E. Wohlfarth, “A mechanism of magnetic hysteresis in heterogeneous alloys,” *Philosophical Transactions of the Royal Society of London. Series A, Mathematical and Physical Sciences*, vol. 240, no. 826, pp. 599–642, 1948.
- [44] M. J. Donahue and M. Donahue, *OOMMF user’s guide, version 1.0*. US Department of Commerce, National Institute of Standards and Technology, 1999.
- [45] M. Beg, R. A. Pepper, and H. Fangohr, “User interfaces for computational science: A domain specific language for oommf embedded in python,” *AIP Advances*, vol. 7, no. 5, p. 056025, 2017.
- [46] F. Pawlek, “Magnetische werkstoffe mit stark temperaturabhängiger sättigungsmagnetisierung,” in *Magnetische Werkstoffe*, pp. 289–291, Springer, 1952.
- [47] J. E. Miltat, M. J. Donahue, *et al.*, “Numerical micromagnetics: Finite difference methods,” *Handbook of magnetism and advanced magnetic materials*, vol. 2, pp. 742–764, 2007.
- [48] M. Weißenhofer and U. Nowak, “Diffusion of skyrmions: the role of topology and anisotropy,” *New Journal of Physics*, vol. 22, no. 10, p. 103059, 2020.
- [49] M. Weißenhofer and U. Nowak, “Orientation-dependent current-induced motion of skyrmions with various topologies,” *Physical Review B*, vol. 99, no. 22, p. 224430, 2019.

VI. APPENDIX

To corroborate the robustness of our results, the HB code of MicroMagnum was checked with simulation software developed by Markus Weisshofer [48, 49]. The resulting annihilation field of a skyrmion configuration ($c_s = 4, a = 0.4 \text{ nm}, M_s = 0.5 \text{ MA/m} \cdot a^3, J = 3 \text{ pJ} \cdot a/n_{\text{nn}}, D = 3 \text{ mJ/m}^2 \cdot a^2/n_{\text{nn}}$ and $K_u = 480 \text{ kJ/m}^3 \cdot a^3$, the sample was $16 \text{ nm} \cdot 16 \text{ nm}$) was in very good agreement (HB simulation in MicroMagnum: $H_{\text{rup}} = 3.62 \text{ T}$, compared to $H_{\text{rup}} = 3.625 \text{ T}$, deviation below 0.15 %). For a more general validation of the HB approach of MicroMagnum see Ref. [25].

To exclude simulation artifacts due to a lack of symmetry breaking in the finite difference methods simulations, the OOP H_{rup} was determined, by simultaneously applying a small, constant IP field, not aligned with any simulation grid axes. Simulations showed that the annihilation field does not vary for small IP fields of several tens of mT. This is an indicator, that our simulations are not dominated by a lack of symmetry breaking, as could occur due to the highly symmetric simulation.

Fig. 9 and 10 show the rupture field and expulsion field, respectively, for all parameter sets presented in Fig. 3.

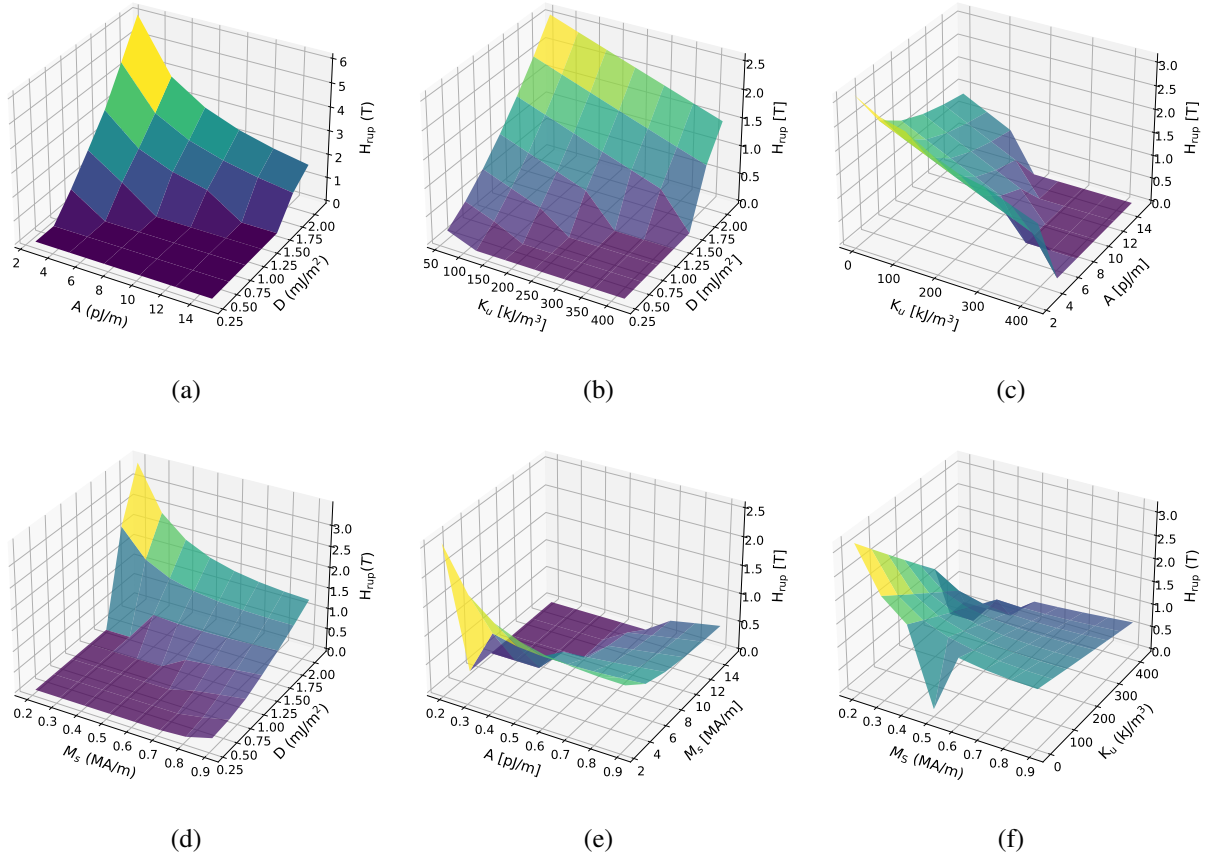


FIG. 9. The rupture field H_{rup} as a function of different magnetic parameters, evaluated in the MS model. The same parameter sets as in Fig. 3 are used. If the configuration was a non-skyrmion configuration, H_{rup} describes the field when the system is homogeneously OOP magnetized. For a detailed discussion on the dependence of every parameter, see Sec. IV B.

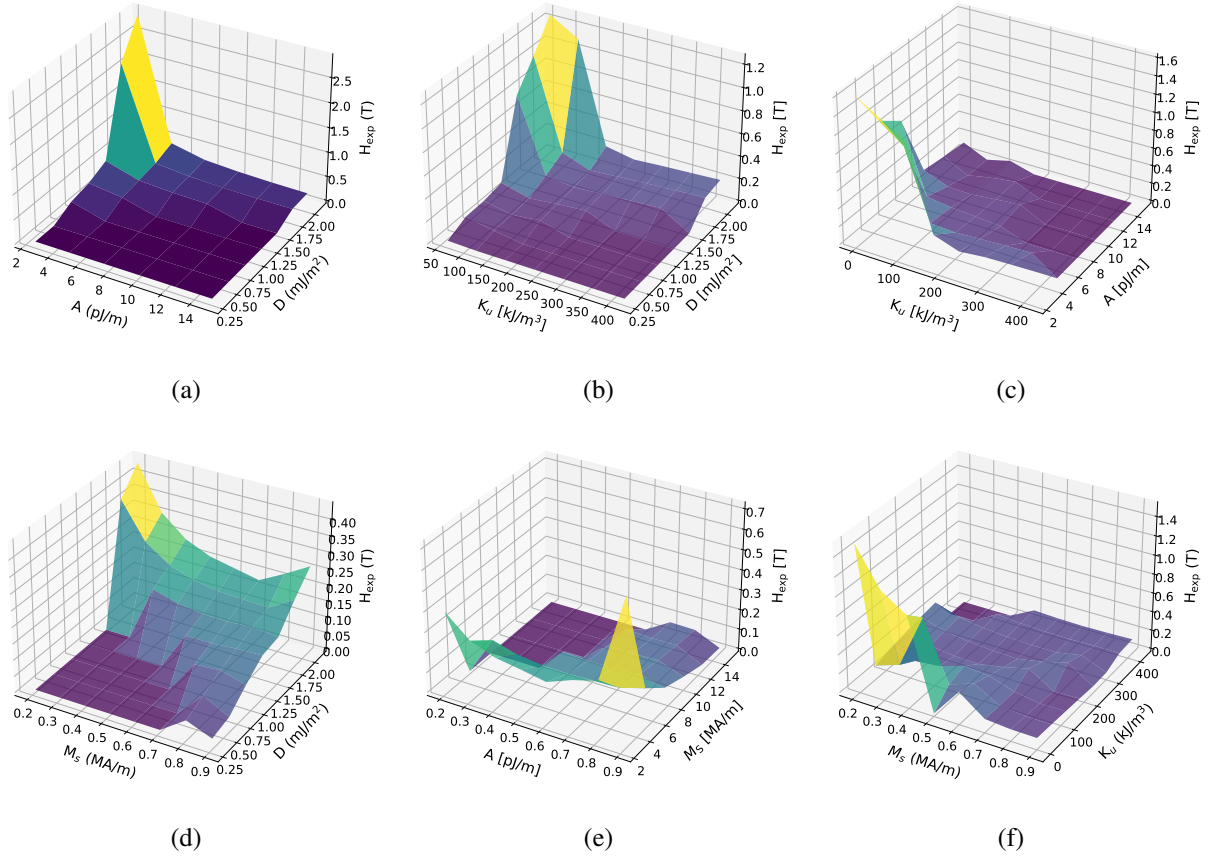


FIG. 10. The expulsion field H_{exp} as a function of different magnetic parameters, evaluated by an MM model with 2 nm lateral cell size. The same parameter sets as in Fig. 3 are used. If the configuration was a non-skyrmion configuration, H_{exp} describes the field when there is no magnetization component in $-z$ direction. For a detailed discussion on the dependence of every parameter, see Sec. IV D. Due to transitions into various magnetic configurations, the dependence is not always as continuous as for the rupture.